analytical chemistry

Article

Cite This: *Anal. Chem.* 2019, 91, 13062−13070

pubs.acs.org/ac

Stability Designs of Cell Membrane Cloaked Magnetic Carbon Nanotubes for Improved Life Span in Screening Drug Leads

Qi Hu,[†,‡] Yusi Bu,[†,‡] Ruiqi Cao,[†,‡] Gao Zhang,[†,‡] Xiaoyu Xie,*[,†,‡] and Sicen Wang*[,†,‡]

[†]School of Pharmacy, Health Science Center, Xi'an Jiaotong University, Xi'an 710061, China

[‡]Shaanxi Engineering Research Center of Cardiovascular Drugs Screening & Analysis, Xi'an 710061, China

Supporting Information

ABSTRACT: Convenient strategies to provide natural cell membranes (CMs)-camouflaged nanomaterials with enhanced stability would prompt the advancement of CMs-coated biomimetic technology and expand the application of these emerging nanomaterials. Herein, we have developed stability-enhanced CMs-camouflaged magnetic carbon nanotubes (MCNTs) to screen drug leads from traditional Chinese medicine (TCMs) that target membrane receptors. By modifying MCNTs with *N*-ethyl-*N*′-(3-(dimethylamino)propyl) carbodiimide hydrochloride (EDC) and *N*-hydroxysuccinimide (NHS), the resulting covalent immobilized CMs-camouflaged MCNTs have improved stability, where the losing amount (20 mg g^{-1}) was significantly decreased compared with that of the unimmobilized materials (40 mg g^{-1}). The high expression ephrinb2/HEK293 cell lines were used to camouflage the EDC/NHS modified MCNTs (CMCNTs) to endow it with drug-screening sites. Moreover, with inherited properties from CMs, ephrinb2/HEK293 CMs-camouflaged CMCNTs possessed good binding capacity and selectivity, and three potential drug leads as mesaconine, deltaline, and 13-dehydroxyindine were screened from *Aconitum carmichaeli Debx*. The pharmacological assays indicated that mesaconine and 13-dehydroxyindine could inhibit cancer cell growth by targeting ephrinb2. As a result, this surface engineering method not only offers an insight into fabrication of stabilized CMs-coated nanomaterials but also inspires more brilliant work in the future and paves the way for the biomimetic functional modification of CNTs for a variety of applications.

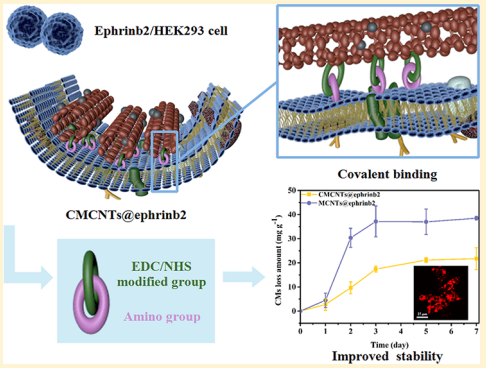

Carbon nanotubes (CNTs) are now regarded as an important focus in academic research and various industrial areas. They have been widely used in hydrogen storage,[1] batteries,[2] drug-delivery systems,[3] antimicrobial treatment,[4] and biosensor diagnostics and analysis[5] because of their excellent mechanical, structural, and electronic properties. In particular, their intrinsic high surface area is one of the most attractive features, which enables them to have excellent adsorption ability.[6] Recently, much progress have been made in exploring functionalization strategies for CNTs to increase the adsorption efficiency in solid-phase extraction (SPE).[7] For example, one of the most recent methods proposes to decorate CNTs with magnetic nanoparticles to simplify the isolation procedure through the magnetic separation technology.[8] However, a stumbling block in the development of SPE is the poor adsorption specificity of CNTs. To increase specific function, a wide range of biomacromolecules, including proteins, antibodies, DNA, and enzymes, could be a promising modality of CNTs functionalization.[9] While a modified strategy for improving specific function has indicated incredible utility for enhancing a selective SPE platform, there is still much room for improvement.

Recently, a natural cell membranes (CMs)-based bioengineering approach has received much attention and has been consequently applied in the development of material biomimetic functionalization.[10−12] As unique natural biomaterials, CMs are superior in many aspects to synthetic biopolymers and single biomacromolecules because of their complete biological structure and complex interface, which cannot be easily replicated in other ways. Zhang et al. have made groundbreaking progress in engineering erythrocyte membrane with functional nanoparticles for many influential biomedical applications, including antitumor therapy,[13,14] blood detoxifcation,[15,16] and immune regulation.[17,18] CMs-coated nanoparticles inherently replicated the highly complex functionalities of the source membrane, bestowing a wide range of properties such as long circulation and specific ligand targeting. Considering the wide range of biological interactions in which natural CMs are involved,[19−21] it can be a promising modality of CNTs functionalization to improve selectivity. It is well-known that CMs have a large number of receptors,[22,23] which are important targets for drug binding and action in vivo. On account of this, CMs-coated CNTs have wide application prospects in screening drug leads. Our group has developed different CMs-camouflaged nanomaterials in order

Received: July 19, 2019
Accepted: September 12, 2019
Published: September 12, 2019

DOI: 10.1021/acs.analchem.9b03268
Anal. Chem. 2019, 91, 13062−13070

to create a completely new platform for drug development. The currently available examples include EGFR/HEK293 CMs-coated magnetic nanoparticles[24] and α_{1A}-AR/HEK293 CMs-camouflaged CNTs[25] for screening drug leads from traditional Chinese medicines (TCMs). Despite the success in camouflaging the nanoparticles with CMs, the serious loss of membrane on the surface of bionic nanomaterials is still a big problem, which makes CMs-coated nanomaterials suffer from short life span and low efficiency. Therefore, it is a fundamental solution to improve the stability of CMs coating through establishing a stronger interaction between the materials and CMs.

Traditionally, the electrostatic interaction and hydrogen bonding between phospholipids and the hydroxyl on the surface of materials are the main force to maintain the stability of membrane coating in the biomimetic functionalization mode.[26−28] These interactions are correspondingly weak and unstable, making the membranes easy to fall off the surface of nanomaterials, which greatly restricts the application of this practical model.[24,25] Therefore, the improvement of the biomimetic nanomaterials' stability has attracted much attention in the past decade. Furthermore, many efforts have been made to enhance the interaction between the nanoparticles and the CM.[29,30] For example, Chen et al. decorated its stationary phase with (3-aminopropyl) triethoxysilane to stabilize the membrane coating.[31] The diimide-activated amidation,[32,33] one of the common methods for covalent immobilizing biomolecules, can significantly enhance the bonding strength and exhibits better biocompatibility. Inspired by this, we reasoned that strategies capable of fine-tuning the interaction between CMs and CNTs might lead to better stability and thus offer rationalizing the design and uses of CMs-camouflaged nanomaterials. Specifically, through the functionalization by *N*-ethyl-*N*′-(3-(dimethylamino)propyl) carbodiimide hydrochloride (EDC) and *N*-hydroxysuccinimide (NHS), active esters on the surface of CNTs can react with the amino groups, which widely exist in the phospholipids of CMs.[34] As a result, the interaction between CMs and nanomaterials is replaced by a covalent bond, rather than hydrophobic or hydrogen interaction, which can greatly improve the stability of bionic nanomaterials.

In this contribution, a stably designed CMs-camouflaged magnetic CNTs has been developed for screening drug leads. Ephrinb2 is a transmembrane ligand for the ephb4 receptor,[35] contributing to the survival, invasion, and migration of tumor cells,[36] and has been proved to be an important drug target in drug lead discovery.[37] Therefore, CMs derived from the high-expression ephrinb2/HEK293 cell lines are used to endow CNTs with good receptor specificity. In contrast to existing CMs-camouflaging systems, we designed an EDC/NHS modified magnetic CNTs to enhance the interaction between CMs and the carriers. The resultant covalent immobilized CMs-camouflaged magnetic CNTs biomimetic materials demonstrate better stability for screening drug leads from a complex matrix because of the low losing amounts of CMs. We anticipate this study will prompt the advancement of CMs-derived biomimetic technology as well as facilitate the biomimetic functional modification of CNTs and expand the application field. In addition, such CMs-coated nanomaterials represent a facile drug-targeting screening platform, which can promote basic research on TCMs materials.

EXPERIMENTAL SECTION

Materials and Regents. CNTs-COOH was purchased from XFNANO material technology Co., Ltd. (Jiangsu, China). Iron(II) sulfate heptahydrate ($FeSO_4·7H_2O$), iron(III) chloride hexahydrate ($FeCl_3·6H_2O$), and ammonium hydroxide (25%) were provided by Guanghua Technology Co., Ltd. (Guangdong, China). RIPA lysis buffer was obtained from Heart Biotechnology Co., Ltd. (WB009; Shaanxi, China). 1,1′-Dioctadecyl-3,3,3′,3′-tetramethylindocarbocyanine perchlorate (DiI) was provided by Beyotime Biotechnology Co., Ltd. (Shanghai, China). Mesaconine, deltaline, and 13-dehydroxyindaconintine were offered by Herbest Biological Technology Co., LTD (Shaanxi, China). Gefitinib, nitrendipine, verapamil, and tamsulosin were provided by Nanjing Ange Pharmaceutical Co., Ltd. (Jiangsu, China). *Aconitum carmichaeli Debx* was offered by the Xi'an medicine market (Shaanxi, China).

Preparation of CMs Biomimetic Materials. The magnetic CNTs-COOH(MCNTs) nanocomposites were fabricated successfully via a modified chemical coprecipitation method according to previously described protocols.[25,38] Then, the carboxylic acid groups of MCNTs were activated by EDC/NHS, forming a stable active ester. Specifically, a suspension of MCNTs (2 mg mL^{-1}) was added to 400 mM NHS in MES (2-(*N*-morpholino)ethanesulfonic acid) buffer and sonicated for 30 min. Under fast stirring, EDC (20 mM) was then added into the mixture, and it was continually stirred for 30 min at room temperature. After that, the mixture was filtrated and washed with distilled water repeatedly to remove residual reagents, and subsequently, it was vacuum-dried at 60 °C for 12 h.

The high-expression ephrinb2/HEK293 cells were cultured in DMEM medium supplemented with 10% fetal bovine serum, 100 mg L^{-1} streptomycin, 100 mg L^{-1} penicillin, and 300 mg L^{-1} G418 at 37 °C in 5% CO_2 atmosphere. The ephrinb2/HEK293 CMs were produced according to a previous report.[25] By hypotonic lysis, mechanical disruption, and centrifugation, the intracellular contents of cells were depleted, and then the CMs were obtained. Meanwhile, the native HEK293 cells without ephrinb2 overexpression were cultured to prepare HEK293-CMs as a control.

To coat CMs onto the surface of EDC/NHS-modified MCNTs (CMCNTs), PBS-containing dispersed MCNTs materials were mixed with CMs by ultrasonication at 4 °C for 10 min. The mixture was subsequently separated using the external magnetic field, and then excess CMs were discarded. BSA was then used to block the nonspecific binding sites on particle surfaces. The ephrinb2/HEK293 CMs-coated CMCNTs (CMCNTs@ephrinb2) were prepared by incubating CMs-cloaked MCNTs with 0.5% BSA in PBS for 10 min at 4 °C. Meanwhile, HEK293-CMs-cloaked MCNTs (CMCNTs@HM) which were camouflaged with native HEK293 CMs without ephrinb2 overexpression and non-CMs-cloaked MCNTs (CMCNTs@NM) which were produced by the same process without CMs were prepared as a comparison.

Characterization of CMs Biomimetic Materials. Membrane camouflaging around the CMCNTs was visualized using Laser scanning confocal microscopy (LSCM; TCS SP8 STED 3X, Leica, Germany) upon staining with DiI (a CMs lipid bilayer label, 549/565 nm, red fluorescence). Transmission electron microscopy (TEM; JEOL JEM-2100Plus, Japan) was used to observe the morphology of obtained materials.

DOI: 10.1021/acs.analchem.9b03268
Anal. Chem. 2019, 91, 13062−13070

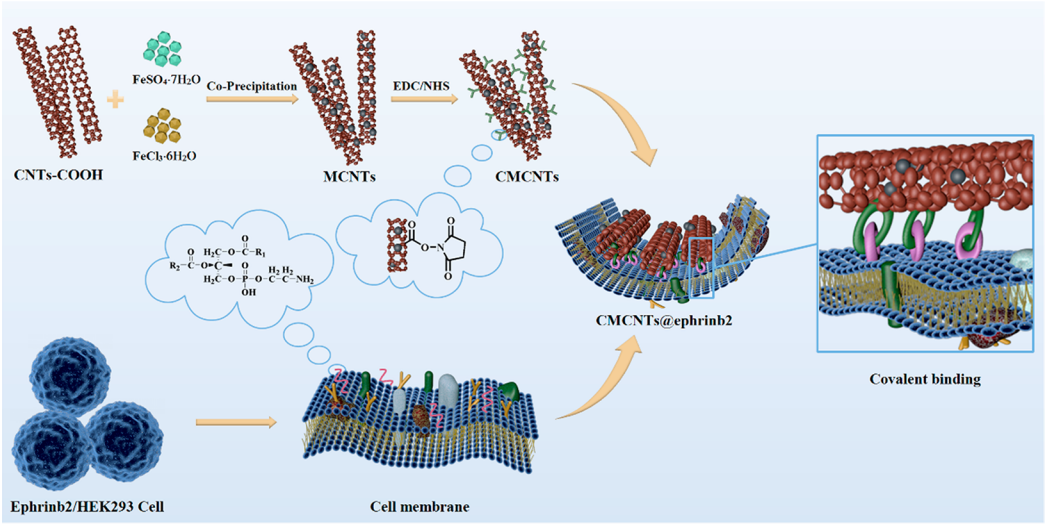

Figure 1. Design of the CMCNTs@ephrinb2 with improved stability.

Magnetic measurements were carried out on vibrating sample magnetometer (VSM; Lake Shore 7307, Ohio, U.S.A.). X-ray photoelectron spectroscopy (XPS; EA3000, Euro Vector, U.S.A.) was performed to clarify the surface element composition of the obtained materials. The crystal phase of the materials was characterized by X-ray diffraction (XRD; D8 Advance, Bruker, Germany) using a Cu Kα source over the scanning range of 2θ = 20−70°. Fourier transform infrared spectroscopy (FTIR) spectra were acquired on the Nicolet Nexus-410 FTIR spectrometer (Madison, U.S.A.) in the range of 4000−400 cm^{-1} to observe the change of functional groups of the obtained materials.

Adsorption Experiments. In order to evaluate the adsorption property of CMCNTs@ephrinb2 on the target compounds, it is essential to investigate the adsorption characteristics by static, dynamic, and selective adsorption experiments. In this study, gefitinib as an ephrinb2 antagonist was used as a positive drug.

In the adsorption isotherm experiments, 5 mg of CMCNTs@ephrinb2, CMCNTs@NM, or CMCNTs@HM was added into 1 mL gefitinib solutions with different concentrations (4 to 1000 mg L^{-1}), respectively. After the adsorption process, the adsorbents were magnetically separated, and the residual amount of gefitinib in supernatant was detected by HPLC. The adsorption capacity of the investigated materials was calculated as eq 1:

$$Q = (C_0 - C_e)V/m \quad (1)$$

In this expression, Q (mg g^{-1}) represents the adsorption capacity of adsorbent. C_0 (mg L^{-1}) and C_e (mg L^{-1}) are the initial and equilibrium concentration of the testing solution, respectively. V (mL) is the volume of testing solution, and m (mg) refers to the amount of the adsorbent.

For the adsorption kinetics, the adsorbents were incubated with 1 mL of gefitinib solution (100 mg L^{-1}). At certain time intervals (1 s−30 min), the residual amount of gefitinib in the supernatant was detected by HPLC. Additionally, the adsorption amount at different time was also estimated by eq 1 with the concentration C_t of the standing time t instead of C_e.

Moreover, to evaluate the selectivity of the obtained materials, four drugs acting on different receptors were selected to conduct the experiments. Briefly, 5 mg of CMCNTs@ephrinb2, CMCNTs@NM, or CMCNTs@HM was added into 100 mg L^{-1} gefitinib (positive drug), nitrendipine, verapamil, and tamsulosin (negative drugs) solutions, respectively. After the adsorption process mentioned above, the remaining amounts of four drugs in the supernatant were measured using HPLC, respectively, and the adsorption capacities were also calculated using eq 1.

Real Application. For potential screening of drug leads, the total extract of *Aconitum carmichaeli Debx* was first prepared by reflux extraction. In brief, 15 g of *Aconitum carmichaeli Debx* was ground to powder and extracted with 70% ethanol (150 mL) for 2 h at 65 °C. The resulting yellowish-brown extraction solution was then filtered to remove the residue, and the filtrate was used for extraction of drug leads using CMCNTs@ephrinb2 as the sorbent. CMCNTs@ephrinb2 (5 mg) was incubated with 1 mL of extract for 10 min. Subsequently, the CMCNTs@ephrinb2 with captured components were collected rapidly using an external magnetic field and washed with 5% acetic acid. Then, the analytes were eluted with DMSO. At last, all solutions were collected and dried by evaporation. The residue was dissolved in methanol and analyzed by HPLC analysis.

Cell Viability Assay. The CCK-8 assay was performed to evaluate the growth-inhibition effects of screened potential drug leads on ephrinb2/HEK293 cells. Cells with a density of 1.5×10^4 cells/well were seeded in 96-well plates and incubated for 24 h to allow cells to sufficiently attach. The cells were then treated with different concentrations of mesaconine, deltaline, and 13-dehydroxyindaconintine for 48 h. After incubation, the culture medium was replaced with serum-free culture medium containing 10 μL of CCK-8 kit solution (YESEN Biotechnology Co., LTD, Shanghai, China) and cultured for 30 min. The absorbance was read at 450 nm by a microplate reader.

Western Blot Analysis. For Western blot analysis, the ephrinb2/HEK293 cells were treated with mesaconine, deltaline, and 13-dehydroxyindaconintine for 48 h, respectively. The total protein extracts were prepared with RIPA lysis buffer, and the protein levels were quantified by BCA protein quantitation kit (Beyotime Biotechnology Co., Ltd., Shanghai, China). Subsequently, proteins were separated by 10% sodium dodecyl sulfate-polyacrylamide gel electrophoresis (SDS-

DOI: 10.1021/acs.analchem.9b03268
Anal. Chem. 2019, 91, 13062−13070

PAGE) and transferred to a nitrocellulose membrane. After they were blocked with 5% nonfat milk, the membranes were incubated with anti-ephrinb2 antibodies (ab150411; Abcam, Cambridge, U.K.) at 1:1000 dilution at 4 °C overnight and then incubated with secondary antibodies conjugated with horseradish peroxidase for 2 h. Finally, the protein bands were detected using ECL reagent (Millipore corporation, Billerica, U.S.A.), and the optical densities of detected proteins were quantified using the LabWork software package.

Molecular Docking Study. A molecular docking test was conducted to study the receptor−inhibitor binding interactions of mesaconine, deltaline, and 13-dehydroxyindaconintine on ephrinb2. Docking calculations were carried out using Surflex-dock module in Sybyl-X2.0. The crystal structure of ephrinb2 (PDB code: 2HLE) was retrieved from the RCSB Protein Data Bank. Water molecules and cocrystallized ligand were removed from the structure, and hydrogen atoms were added during protein preparation. The structures of docking compounds gefitinib, mesaconine, deltaline, and 13-dehydroxyindaconintine were depicted with chemdraw and followed by the structural energy optimization using Powell's method.

RESULTS AND DISCUSSION

Preparation of CMCNTs@ephrinb2. As shown in Figure 1, we described a strategy to covalently immobilize the CMs on the surface of MCNTs in order to fabricate stability-enhanced drug targeting discovery nanomaterials. CMs-derived nanomaterials have been previously demonstrated in many systems. However, these biomimetic materials suffered from poor stability, resulting in limited life span and low reproducibility, which has greatly hindered the CMs-derived nanomaterials from being widely used. Herein, we used EDC/NHS to modify MCNTs preparing CMCNTs, which were rich in active ester. Meanwhile, high-expression ephrinb2/HEK293 cell membrane fragments were prepared using a previously published protocol, which were composed of phospholipid bilayer, offering abundant free amino groups. Subsequently, the CMCNTs@ephrinb2 were synthesized through covalent binding between the active esters of CMCNTs and the amino groups from the CMs. After that, CMCNTs@ephrinb2 were added to screen the potential drug leads that can bind the ephrinb2 receptors from TCMs.

In order to obtain more effective CMCNTs@ephrinb2 with more active sites, several preparation conditions were investigated, including the initial concentration of CMs and the incubation time. First, the CMs concentration was modulated to obtain the optimal drug-adsorption materials. As illustrated in Table S1, the optimal concentration of CMs was 5 mg mL^{-1}. Next, the incubation time was also an important factor. By varying the incubation time (1, 10, and 60 min), a series of materials were fabricated, and the results of CMs binding amounts indicate that the optimal time was 10 min.

Most importantly, as bioactive-compound-adsorption materials, CMCNTs@ephrinb2 was supposed to be more stable and efficient. First, in order to verify the stability of the materials, the losing amounts of CMs coating within 7 days were evaluated. As shown in Figure 2A, the results showed that the losing amounts of CMs coating on CMCNTs was 20 mg g^{-1}, while the losing amounts on MCNTs was almost 40 mg g^{-1}. This indicated that the immobilized CMCNTs@ephrinb2 showed higher stability than the unimmobilized MCNTs@ephrinb2, which proved the enhanced interaction between the

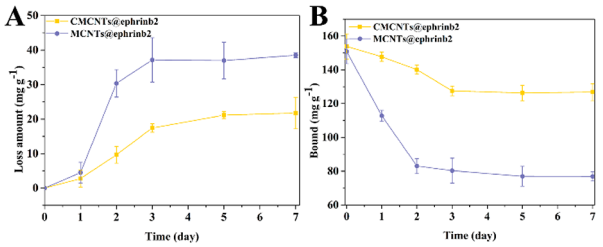

Figure 2. (A) CMs losing amount and (B) adsorption capacity of CMCNTs@ephrinb2 and MCNTs@ephrinb2 after different days (4 °C).

modified MCNTs and CMs. Second, to further investigate the reproducibility of the materials, the adsorption capacities of CMCNTs@ephrinb2 and MCNTs@ephrinb2 after different days were compared. It was seen in Figure 2B that there was little difference in adsorption capacity between the two materials at the beginning, which was due to the similar coating amount of CMs on the surface of CNTs. However, with the increase of time, the adsorption capacity of CMCNTs@ephrinb2 decreased little, while that of MCNTs@ephrinb2 exhibited a significant decrease, which was due to the weakness and instability of traditional binding interactions, making the membranes easy to fall off the surface of nanomaterials. This result indicated that EDC/NHS modification could improve the stability of CMs coating, demonstrating the validity of the covalent immobilization strategy.

Characterization of CMCNTs@ephrinb2. To visually validate the successful coating with CMs, LSCM imaging was performed. The CMCNTs@ephrinb2 was incubated with DiI (dissolved in ethanol) at 4 °C for 40 min and then washed with PBS for three times to remove excess dye. Meanwhile, the CMCNTs@NM was treated in the same way. Finally, the LSCM images were obtained under 549 nm excitation light source. As shown in Figure 3A, the presence of membrane phospholipids on the surface of CMCNTs@ephrinb2 was obviously observed in visual field (e,f). By contrast, the red fluorescence was hardly monitored in CMCNTs (b,c), demonstrating the successful coating of CMs on the surface of CMCNTs.

Moreover, the microstructures of CNTs-COOH and CMCNTs@ephrinb2 were explored by TEM, and the images were given in Figure 3B. It was clear that the CNTs-COOH was decorated by many obvious spherical Fe_3O_4 nanoparticles and that uniform CMs was coated on the surface of CMCNTs (Figure 3Bb).

In order to explore the magnetic properties, VSM was applied to record the magnetic behavior of Fe_3O_4 (Figure 3Ca), MCNTs (Figure 3Cb), and CMCNTs@ephrinb2 (Figure 3Cc). The saturation magnetization (Ms) values of MCNTs and CMCNTs@ephrinb2 were 32 and 24 emu g^{-1}, respectively, which were lower than that of Fe_3O_4 (71 emu g^{-1}). The decrease of Ms value could be ascribed to the existence of CNTs-COOH and CMs, which reduced the content of Fe_3O_4 of the composites. With this adequate magnetic property, CMCNTs@ephrinb2 could be used as a promising adsorbent for biological and functional application as it can be separated rapidly by an extra magnetic field. Overall, these results confirmed the adequate magnetism of CMCNTs@ephrinb2, making them can be separated rapidly through an applied magnetic field.

DOI: 10.1021/acs.analchem.9b03268
Anal. Chem. 2019, 91, 13062−13070

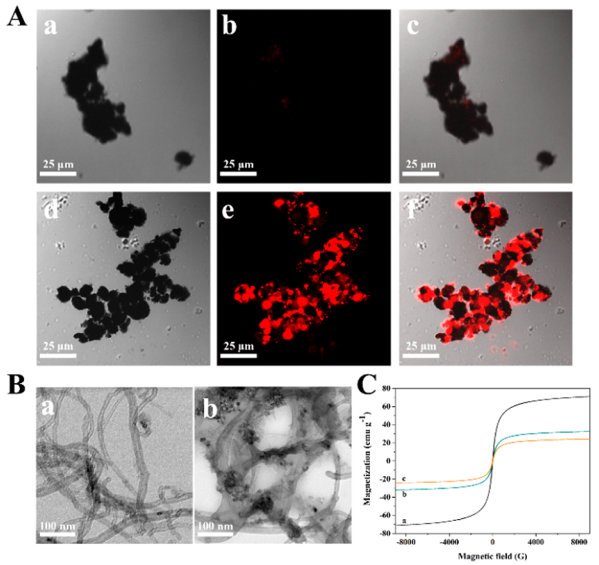

Figure 3. (A) LSCM images of CMCNTs (a, b, and c) and CMCNTs@ephrinb2 (d, e, and f): (a and d) were bright field; (b and e) were excited at 549 nm to observe DiI-dyed CMs; (c) was merged by (a) and (b); (f) was merged by (c) and (d). The red fluorescence indicated DiI-dyed CMs; (B) TEM images of CNTs-COOH (a) and CMCNTs@ephrinb2 (b); (C) Magnetic hysteresis loops of Fe_3O_4 (a), MCNTs (b), and CMCNTs@ephrinb2 (c).

In addition, XPS measurements were conducted to investigate the elements and surface groups of Fe_3O_4, CNTs-COOH, MCNTs, and CMCNTs@ephrinb2. As shown in Figure S1, the Fe 2p peak appeared in MCNTs (curve (c)) compared with Fe_3O_4 (curve (a)) and CNTs-COOH (curve (b)), confirming the successful decoration of Fe_3O_4 on the surface of CNTs-COOH. Furthermore, after being coated with CMs, the peaks of N 1s and P 2p in curve (d) were obviously observed, corresponding to the nitrogen and phosphorus elements of CMs, respectively, which demonstrated the successful preparation of CMCNTs@ephrinb2.

To understand the crystal structures of Fe_3O_4, CNTs-COOH, MCNTs, and CMCNTs@ephrinb2, XRD were carried out, and the results were depicted in Figure S2. As shown in curve b, the wide diffraction peak at 26.4° was assigned to the (002) planes of CNTs-COOH. Besides, the diffraction peaks at $2\theta = 30.3°$, 35.6°, 43.3°, 53.7°, 57.4°, and 62.7° observed in curve a, represented the reflection from (220), (311), (400), (422), (511), and (440) planes of the structure of Fe_3O_4 (JCPDS No. 65-3107). After growth of Fe_3O_4 on the CNTs-COOH surfaces, it can be found that the typical diffraction peaks of CNTs-COOH and Fe_3O_4 existed together in MCNTs (curve c) and CMCNTs@ephrinb2 (curve d), which demonstrated that the Fe_3O_4 nanoparticles were successfully attached on the CNTs-COOH.

Furthermore, the FTIR spectra of CMCNTs (curve a) and CMCNTs@ephrinb2 (curve b) were displayed in Figure S3. The peak at 1727 cm^{-1} (curve a) was assigned to the stretching vibration of C−O. After being camouflaged with CMs, significant changes were observed (curve b). The band at 1727 cm^{-1} disappeared, and the bands at 1627 and 1439 cm^{-1} can be observed, which were assigned to the stretching vibration of C−O and C−N in CMCNTs@ephrinb2, respectively, confirming that the amide bond was formed between the CMs and CMCNTs. Moreover, the intensity decrease of 580 cm^{-1} band further proved that CMs were coated on the surface of functionalized CNTs.

Adsorption Capacity. Adsorption isotherms represent the adsorption capacity of the adsorbents to gefitinib. The relationship between adsorption capacity of CMCNTs@ephrinb2, CMCNTs@NM, and CMCNTs@HM and the initial concentration were depicted in Figure 4A. It could be

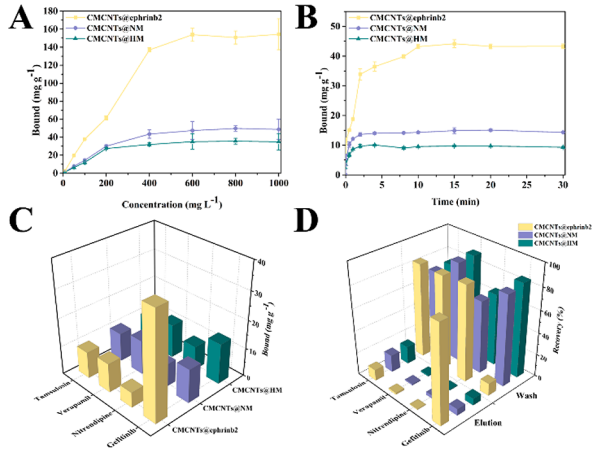

Figure 4. (A) Static adsorption isotherm curves of CMCNTs@ephrinb2, CMCNTs@NM, and CMCNTs@HM after incubation at 4 °C for 20 min; (B) dynamic adsorption curves of CMCNTs@ephrinb2, CMCNTs@NM, and CMCNTs@HM after incubation with gefitinib at 4 °C; (C) total adsorption capacity of CMCNTs@ephrinb2, CMCNTs@NM, and CMCNTs@HM toward four drugs; (D) the recovery of four drugs during the washing and elution process.

discovered that the adsorption capacity of three adsorbents increased dramatically with the increase of the gefitinib concentration (4−1000 mg L^{-1}) and then reached saturation at 600 mg L^{-1}. Furthermore, the adsorption capacity of CMCNTs@ephrinb2, CMCNTs@NM, and CMCNTs@HM were 153.8, 49.7, and 35.6 mg g^{-1}, respectively. The result demonstrated that larger amounts of gefitinib were adsorbed on CMCNTs@ephrinb2 than the other adsorbents, which could be due to the larger amounts of specific receptors on the surface of CMCNTs@ephrinb2.

In order to analyze the adsorption properties of adsorbents and achieve the maximum adsorption, Freundlich, Langmuir, Scatchard, and Dubinin−Radushkevich isotherms were used to fit the above data (Table 1). On the basis of the values of correlation coefficient (r), the adsorption behavior was more in line with the Langmuir model, suggesting a monolayer sorption of gefitinib on the surface of prepared adsorbents.[39]

Adsorption Kinetics. Adsorption kinetics experiments were carried out to depict the dynamic adsorption characteristics of CMCNTs@ephrinb2, CMCNTs@NM, and CMCNTs@HM. As Figure 4B illustrated, the adsorption of gefitinib rose significantly in the first 4 min. This was due to abundant binding sites on the adsorbent surface, promoting the combination of adsorbent and gefitinib. Over time, the adsorption rate decreased, as the remaining binding sites were limited and hard to be occupied. Gradually, adsorption equilibrium was reached at approximately 10 min. Meanwhile, CMCNTs@ephrinb2 presented larger adsorption values than CMCNTs@NM and CMCNTs@HM.

DOI: 10.1021/acs.analchem.9b03268
Anal. Chem. 2019, 91, 13062−13070

Table 1. Equations and Parameters of Adsorption Isotherms of CMCNTs@ephrinb2, CMCNTs@NM, and CMCNTs@HM

isotherm model	equation and parameters	CMCNTs@ephrinb2	CMCNTs@NM	CMCNTs@HM
Freundlich	$lgQ_e = lgK_F + mlgC_e$			
	K_F (L mg^{-1})	0.2868	0.2583	0.2337
	m	0.9809	0.8208	0.7931
	r	0.8845	0.8854	0.8783
Langmuir	$\frac{C_e}{Q_e} = \frac{1}{Q_{max}K_L} + \frac{1}{Q_{max}}C_e$			
	K_L (L mg^{-1})	0.0007	0.0032	0.0048
	Q_{max} (mg g^{-1})	434.78	62.50	39.53
	r	0.9774	0.9427	0.9590
Dubinin−Radushkevich	$lgT_e = lgT_{max} - K_{ad}\left(RTlg\left(1 + \frac{1}{C_e}\right)\right)^2$			
	K_{ad} (mg^2 kJ^{-2})	1.6×10^{-5}	1.3×10^{-5}	1.3×10^{-5}
	Q_s (mg g^{-1})	66.86	24.40	19.13
	r	0.8606	0.8431	0.8513
Scatchard	$\frac{Q_e}{C_e} = \frac{Q_{max} - Q_e}{K_d}$			
	K_d (mg L^{-1})	2114.16	523.29	434.78
	Q_{max} (mg g^{-1})	662.65	89.05	62.17
	r	0.3618	0.8911	0.8138

Furthermore, the kinetic data were simulated by the pseudo-first-order (PFO) and pseudo-second-order (PSO) models (Table S2). It clearly indicated that PSO model possessed a higher linear regression r of CMCNTs@ephrinb2, CMCNTs@NM, and CMCNTs@HM than that of PFO model. This result indicated that the adsorption process was dominated by chemisorption,[40] which could be due to the hydrogen bond interaction between gefitinib and the receptors.

Adsorption Selectivity. High selectivity of CMCNTs@ephrinb2 was crucial to practical application. To evaluate the adsorption selectivity of CMCNTs@ephrinb2, CMCNTs@NM, and CMCNTs@HM, four different drugs (gefitinib, nitrendipine, verapamil, and tamsulosin) at an initial concentration of 100 mg L^{-1} were used. These drugs were chosen because they are known to act on different receptors. It is clear that the adsorption of gefitinib by CMCNTs@ephrinb2 was much higher than that of other drugs (Figure 4C) and was difficult to be desorbed during the washing process (Figure 4D). However, there was no significant difference in the adsorption capacity of CMCNTs@NM and CMCNTs@HM for the four drugs (Figure 4C). In addition, the adsorbed components of CMCNTs@NM and CMCNTs@HM can be almost completely desorbed during the washing process (Figure 4D), which can be attributed to nonspecific interactions between CMCNTs@NM and CMCNTs@HM with the drugs. These results demonstrated that the CMCNTs@ephrinb2 possessed a superior selectivity.

Optimization Parameters of the SPE Procedure. The appropriate eluent, elution volume, and elution time for SPE procedure were evaluated in single-factor experiments. And all tests were performed in triplicate.

It is fundamental that selecting the most suitable washing and elution solutions for desorption in the SPE process. Different kinds of solutions were tested, including water, water−methanol (9:1, v/v), 0.1% acetic acid, 2% acetic acid, 5% acetic acid, and DMSO. Figure 5A graphically displayed the desorption yields of gefitinib and compared the effect of different solutions. Significant differences were observed in the recoveries of gefitinib depending on solution type. It was found that 5% acetic acid only exhibited a high desorption yield for CMCNTs@NM, while DMSO displayed a high desorption yield for both CMCNTs@ephrinb2 and CMCNTs@NM. Thus, 5% acetic acid and DMSO were chosen as the washing and elution solution, respectively.

The proper volume of eluent was an important parameter for higher desorption efficiency. The optimization of volume (0.5, 1, 4, and 5 mL) was shown in Figure 5B. The recovery of gefitinib for CMCNTs@ephrinb2 reached a maximum (78.8%) when extracted with 1 mL of DMSO. However, it could be seen that there was no significant difference in the desorption yield for CMCNTs@NM with the volume increased. Accordingly, 1 mL was selected for the following experiment.

Furthermore, to determine the optimal elution time, different time (0.08, 0.17, 0.5, 1, 2, 5, 10, and 20 min) was employed. As displayed in Figure 5C, the recovery increased significantly up to 5 min. A further increase in the elution time to 20 min had no significant difference on the desorption efficiency. As a result, an elution time of 5 min was therefore chosen as the optimum condition.

Method Validation and Application in TCMs Samples. To assess the performance of the proposed method, validation experiments were performed, including the linearity range, limit of detection (LOD), precision, and accuracy. The test range of linearity was 0.1−600 mg L^{-1} with r = 0.9993, and the LOD (S/N = 3) was 0.5×10^{-3} mg L^{-1}. In particular, the life span of the biological adsorbent was an important property in practical application. Thus, the reproducibility was investigated, in which relative standard deviation (RSD) as an evaluation indicator was tested for the interday precision. The results exhibited that the RSD of CMCNTs@ephrinb2 and MCNTs@ephrinb2 were 3.4% and 12.8%, respectively, demonstrating better reproducibility and stability of CMCNTs@ephrinb2, which was fully benefited from the covalent immobilization strategy.

DOI: 10.1021/acs.analchem.9b03268
Anal. Chem. 2019, 91, 13062−13070

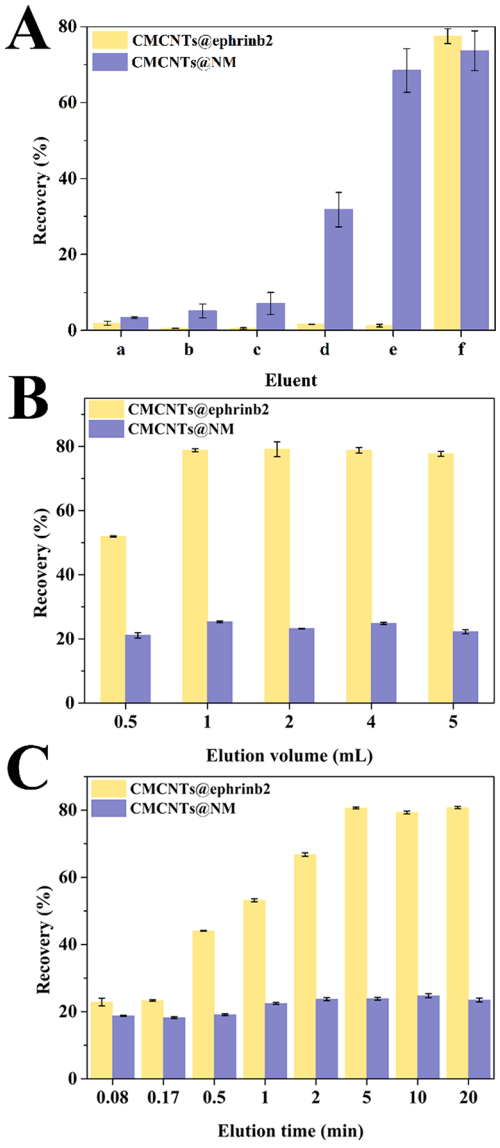

Figure 5. Optimization of SPE procedure. (A) Selection of washing and elution solution: water (a), water−methanol (9:1, v/v) (b), 0.1% acetic acid (c), 2% acetic acid (d), 5% acetic acid (e), and DMSO (f); (B) Elution volume; (C) Elution time.

The obtained CMCNTs@ephrinb2 was applied to provide a quick and targeted drug-discovery technique. Hence, it was used to screen drug leads from extract samples of *Aconitum carmichaeli Debx*. From Figure 6, we can conclude that most components of extract samples have less affinity on the CMCNTs@ephrinb2 model. After washing and eluting, a total of three components were observed in the elution, which ought to be the potential active components enriched by CMCNTs@ephrinb2. Furthermore, above three active components were preliminarily identified as mesaconine, deltaline, and 13-dehydroxyindine by TOFMS. Then, the standard solutions were applied to verify the inference, and the results were in accordance with the experiment results.

Pharmacological Effect. Because of above three components were likely to interact with ephrinb2/HEK293 CMs, a cell viability assay was performed to confirm the inhibitory effect on ephrinb2/HEK293 cell proliferation by CCK-8 agent. As depicted in Figure 7A, with the concentration of mesaconine, deltaline, and 13-dehydroxyindine increased (1.57 to 50 μg mL^{-1}), the inhibitory activity on ephrinb2/HEK293 cell proliferation increased in a dose-dependent manner. The half-maximal inhibitory concentrations (IC_{50}) of mesaconine, deltaline, and 13-dehydroxyindine were 12.56, 17.71, and 13.35 μg mL^{-1}, respectively. It could be concluded that the screened compounds were selectively acting on ephrinb2/HEK293 CMs.

In order to further assess whether mesaconine, deltaline, and 13-dehydroxyindine could regulate the ephrinb2 pathway, the Western blot assay was carried out. The results showed that expression of ephrinb2 was strongly decreased by mesaconine and 13-dehydroxyindine in ephrinb2/HEK293 cells (Figure 7B,C), indicating that two screened compounds could inhibit cell growth by targeting ephrinb2. Although deltaline inhibited cell proliferation in a dose-dependent manner, it exhibited weak inhibition effect on the ephrinb2 expression. It could be inferred that deltaline may not inhibit ephrinb2/HEK293 cell proliferation through the ephrinb2 signaling pathway.

Interaction Simulations of Screened Components with Ephrinb2. To investigate the underlying interaction mechanism, docking studies were performed to explore the interaction of mesaconine, deltaline, and 13-dehydroxyindine with the active site of ephrinb2 (PDB ID: 2HLE). The docking results were manually checked to ensure that the binding mode of the compound had reasonable interaction and geometry

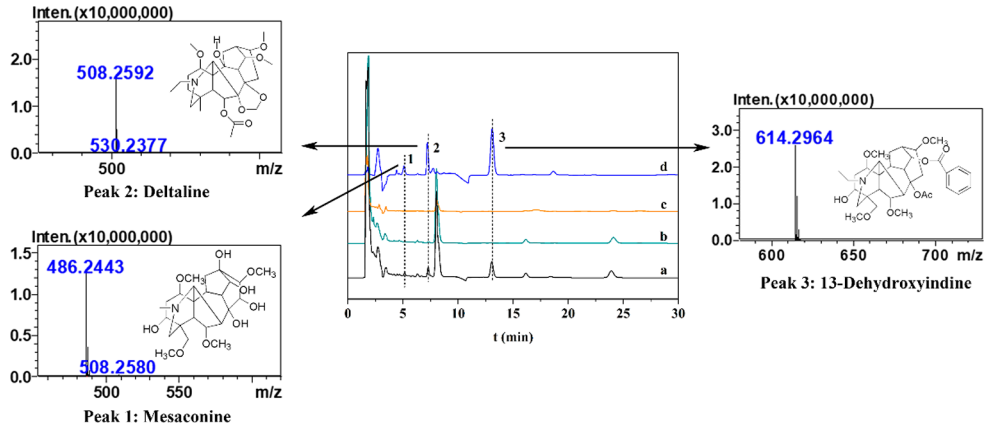

Figure 6. Chromatograms of the practical application using CMCNTs@ephrinb2. Initial solution (a), solution after loading (b), solution after washing (c), and solution after eluting (d) and TOFMS results of the peak 1, peak 2, and peak 3.

DOI: 10.1021/acs.analchem.9b03268
Anal. Chem. 2019, 91, 13062−13070

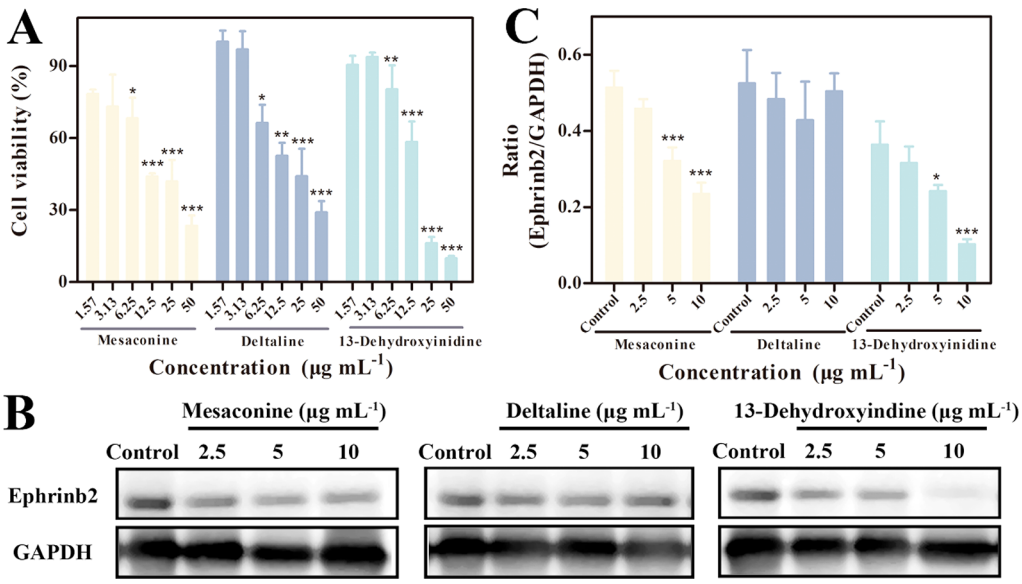

Figure 7. (A) Effect of mesaconine (a), deltaline (b), and 13-dehydroxyindine (c) on the cell growth of ephrinb2/HEK293 cells after 48 h incubation; (B) The inhibitory effect of mesaconine (a), deltaline (b), and 13-dehydroxyindine (c) on ephrinb2 expression; (C) The results were quantified by densitometry analysis and normalization to GAPDH (*p < 0.05, **p < 0.01, ***p < 0.001).

fitting. As we can see, both mesaconine (Figure S4B) and 13-dehydroxyindine (Figure S4D) formed three hydrogen bonds with the active site of ephrinb2 and showed better hydrogen bonding than deltaline (Figure S4C), which were accordance with the above pharmacological results.

CONCLUSIONS

In summary, we have successfully designed a stability-enhanced CMs-camouflaged nanomaterials CMCNTs@epheinb2 for screening drug leads targeting membrane receptor from TCMs. Through the EDC/NHS modification, CMs can be covalently anchored on the surface of MCNTs while still maintaining its inherent nature. This procedure results in enhanced membrane coating stability, prolonged life span as well as better performance of reproducibility. Along with inherited properties from CMs, the developed CMCNTs@epheinb2 was successfully applied for potential screening of drug leads from *Aconitum carmichaeli Debx* with high sensitivity and selectivity. In summary, our covalent immobilization strategy improved the stability of the biomimetic nanomaterials while maintaining the original features of the natural CMs. This platform approach not only provided alternative solution for the rational design of improved biomimetic nanomaterials but also facilitated the biomimetic functional modification of carbon nanotubes.

ASSOCIATED CONTENT

Supporting Information

The Supporting Information is available free of charge on the ACS Publications website at DOI: 10.1021/acs.analchem.9b03268.

XPS patterns of Fe_3O_4, CNTs-COOH, MCNTs, and CMCNTs@ephrinb2; XRD patterns of Fe_3O_4, CNTs-COOH, MCNTs, and CMCNTs@ephrinb2; the binding model of compounds gefitinib, mesaconine, deltaline, and 13-dehydroxyindine with ephrinb2 (PDB ID: 2HLE); materials' compositions of a cell membrane coated on CMCNTs; kinetic parameters for adsorption of gefitinib onto CMCNTs@ephrinb2, CMCNTs@NM, and CMCNTs@HM (PDF)

AUTHOR INFORMATION

Corresponding Authors

*Tel.: +86 29 82656788. E-mail: xiexiaoyu@xjtu.edu.cn (X. Xie).

*Tel.: +86 29 82656788. E-mail: wangsc@mail.xjtu.edu.cn (S. Wang).

ORCID

Xiaoyu Xie: 0000-0003-3936-3565

Sicen Wang: 0000-0002-2757-3277

Author Contributions

S.C.W. and X.Y.X. designed the project and provided overall guidance. Q.H. carried out the experiments, analyzed data and wrote the paper. Y.S.B., R.Q.C., and G.Z. analyzed data and edited the article. All authors reviewed the manuscript.

Notes

The authors declare no competing financial interest.

ACKNOWLEDGMENTS

We gratefully acknowledge the National Natural Science Foundation of China (Nos. 81503033 and 81673398), the Fundamental Research Funds for the Central Universities (No. xjj2018222) for financial support, and the World-Class Universities (Disciplines) and the Characteristic Development Guidance Funds for the Central Universities (No. PY3A012) for financial support. We thank Dr. Hao, Dr. Chang, and Dr. Huang at instrument Analysis Center of Xi'an Jiaotong University for their assistance with LSCM, XPS, and XRD analysis.

REFERENCES

(1) Liu, M. J.; Xiao, X. Z.; Zhao, S. C.; Chen, M.; Mao, J. F.; Luo, B. S.; Chen, L. X. *J. Mater. Chem. A* **2019**, *7*, 5277−5287.

(2) Yu, X. F.; Tian, D. X.; Li, W. C.; He, B.; Zhang, Y.; Chen, Z. Y.; Lu, A. H. *Nano Res.* **2019**, *12*, 1193−1197.

DOI: 10.1021/acs.analchem.9b03268
Anal. Chem. 2019, 91, 13062−13070

(3) Fabbro, C.; Ali-Boucetta, H.; Da Ros, T.; Kostarelos, K.; Bianco, A.; Prato, M. *Chem. Commun.* **2012**, *48*, 3911−3926.
(4) Liu, S. B.; Ng, A. K.; Xu, R.; Wei, J.; Tan, C. M.; Yang, Y. H.; Chen, Y. A. *Nanoscale* **2010**, *2*, 2744−2750.
(5) Lee, J.; Morita, M.; Takemura, K.; Park, E. Y. *Biosens. Bioelectron.* **2018**, *102*, 425−431.
(6) Abdi, J.; Vossoughi, M.; Mahmoodi, N. M.; Alemzadeh, I. *Chem. Eng. J.* **2017**, *326*, 1145−1158.
(7) Sitko, R.; Zawisza, B.; Malicka, E. *TrAC, Trends Anal. Chem.* **2012**, *37*, 22−31.
(8) Liu, Y. Z.; Guo, L. R.; Huang, H. Y.; Dou, J. B.; Huang, Q.; Gan, D. F.; Chen, J. Y.; Li, Y. X.; Zhang, X. Y.; Wei, Y. *J. Colloid Interface Sci.* **2019**, *545*, 8−15.
(9) Adeli, M.; Soleyman, R.; Beiranvand, Z.; Madani, F. *Chem. Soc. Rev.* **2013**, *42*, 5231−5256.
(10) Fang, R. H.; Kroll, A. V.; Gao, W.; Zhang, L. *Adv. Mater.* **2018**, *30*, 1706759.
(11) Hu, C. M. J.; Fang, R. H.; Wang, K. C.; Luk, B. T.; Thamphiwatana, S.; Dehaini, D.; Nguyen, P.; Angsantikul, P.; Wen, C. H.; Kroll, A. V.; Carpenter, C.; Ramesh, M.; Qu, V.; Patel, S. H.; Zhu, J.; Shi, W.; Hofman, F. M.; Chen, T. C.; Gao, W. W.; Zhang, K.; Chien, S.; Zhang, L. F. *Nature* **2015**, *526*, 118−121.
(12) Zhen, X.; Cheng, P. H.; Pu, K. Y. *Small* **2019**, *15*, 1804105.
(13) Li, J. C.; Zhen, X.; Lyu, Y.; Jiang, Y. Y.; Huang, J. G.; Pu, K. Y. *ACS Nano* **2018**, *12*, 8520−8530.
(14) Sun, H.; Su, J.; Meng, Q.; Yin, Q.; Chen, L.; Gu, W.; Zhang, P.; Zhang, Z.; Yu, H.; Wang, S.; Li, Y. *Adv. Mater.* **2016**, *28*, 9581−9588.
(15) Chen, H.-W.; Fang, Z.-S.; Chen, Y.-T.; Chen, Y.-I.; Yao, B.-Y.; Cheng, J.-Y.; Chien, C.-Y.; Chang, Y.-C.; Hu, C.-M. J. *ACS Appl. Mater. Interfaces* **2017**, *9*, 39953−39961.
(16) Wu, Z.; Li, T.; Gao, W.; Xu, T.; Jurado-Sanchez, B.; Li, J.; Gao, W.; He, Q.; Zhang, L.; Wang, J. *Adv. Funct. Mater.* **2015**, *25*, 3881−3887.
(17) Wei, X.; Gao, J.; Fang, R. H.; Luk, B. T.; Kroll, A. V.; Dehaini, D.; Zhou, J.; Kim, H. W.; Gao, W.; Lu, W.; Zhang, L. *Biomaterials* **2016**, *111*, 116−123.
(18) Fontana, F.; Shahbazi, M. A.; Liu, D. F.; Zhang, H. B.; Makila, E.; Salonen, J.; Hirvonen, J. T.; Santos, H. A. *Adv. Mater.* **2017**, *29*, 1603239.
(19) Chen, X.; Cao, Y.; Lv, D.; Zhu, Z.; Zhang, J.; Chai, Y. *J. Chromatogr. A* **2012**, *1242*, 67−74.
(20) Chen, X.; Cao, Y.; Zhang, H.; Zhu, Z.; Liu, M.; Liu, H.; Ding, X.; Hong, Z.; Li, W.; Lv, D.; et al. *Anal. Chem.* **2014**, *86*, 4748−4757.
(21) Zheng, L.; Chen, S.; Cao, Y.; Zhao, L.; Gao, Y.; Ding, X.; Wang, X.; Gu, Y.; Wang, S.; Zhu, Z.; et al. *J. Chromatogr. A* **2018**, *1564*, 145−154.
(22) Drews, J. *Science* **2000**, *287*, 1960−1964.
(23) Patching, S. G. *Biochim. Biophys. Acta, Biomembr.* **2014**, *1838*, 43−55.
(24) Bu, Y.; Hu, Q.; Ke, R.; Sui, Y.; Xie, X.; Wang, S. *Chem. Commun.* **2018**, *54*, 13427−13430.
(25) Hu, Q.; Bu, Y.; Zhen, X.; Xu, K.; Ke, R.; Xie, X.; Wang, S. *Chem. Eng. J.* **2019**, *364*, 269−279.
(26) Luk, B. T.; Hu, C.-M. J.; Fang, R. H.; Dehaini, D.; Carpenter, C.; Gao, W.; Zhang, L. *Nanoscale* **2014**, *6*, 2730−2737.
(27) Hu, C.-M. J.; Zhang, L.; Aryal, S.; Cheung, C.; Fang, R. H.; Zhang, L. *Proc. Natl. Acad. Sci. U. S. A.* **2011**, *108*, 10980−10985.
(28) Wang, S.; Sun, M.; Zhang, Y.; Du, H.; He, L. *J. Chromatogr. A* **2010**, *1217*, 5246−5252.
(29) Yadavalli, S. S.; Xiao, Q.; Sherman, S. E.; Hasley, W. D.; Klein, M. L.; Goulian, M.; Percec, V. *Proc. Natl. Acad. Sci. U. S. A.* **2019**, *116*, 744−752.
(30) He, Y.; Li, R.; Li, H.; Zhang, S.; Dai, W.; Wu, Q.; Jiang, L.; Zheng, Z.; Shen, S.; Chen, X.; Zhu, Y.; Wang, J.; Pang, Z. *ACS Nano* **2019**, *13*, 4148−4159.
(31) Ding, X.; Cao, Y.; Yuan, Y.; Gong, Z.; Liu, Y.; Zhao, L.; Lv, L.; Zhang, G.; Wang, D.; Jia, D.; Zhu, Z.; Hong, Z.; Chen, X.; Chai, Y. *Anal. Chem.* **2016**, *88*, 12081−12089.
(32) Jiang, K. Y.; Schadler, L. S.; Siegel, R. W.; Zhang, X. J.; Zhang, H. F.; Terrones, M. *J. Mater. Chem.* **2004**, *14*, 37−39.
(33) Asuri, P.; Karajanagi, S. S.; Sellitto, E.; Kim, D.-Y.; Kane, R. S.; Dordick, J. S. *Biotechnol. Bioeng.* **2006**, *95*, 804−811.
(34) Veatch, S. L.; Keller, S. L. *Phys. Rev. Lett.* **2002**, *89*, 268101.
(35) Yang, D.; Jin, C. N.; Ma, H.; Huang, M. Y.; Shi, G. P.; Wang, J. N.; Xiang, M. X. *Angiogenesis* **2016**, *19*, 297−309.
(36) Sawamiphak, S.; Seidel, S.; Essmann, C. L.; Wilkinson, G. A.; Pitulescu, M. E.; Acker, T.; Acker-Palmer, A. *Nature* **2010**, *465*, 487−491.
(37) Ma, W.; Zhu, M.; Zhang, D.; Yang, L.; Yang, T.; Li, X.; Zhang, Y. *Phytomedicine* **2017**, *25*, 45−51.
(38) Xie, X.; Hu, Q.; Ke, R.; Zhen, X.; Bu, Y.; Wang, S. *Chem. Eng. J.* **2019**, *371*, 130−137.
(39) Zhang, J.; Yan, X.; Hu, X.; Feng, R.; Zhou, M. *Chem. Eng. J.* **2018**, *347*, 640−647.
(40) Tang, J.; Li, Y.; Wang, X.; Daroch, M. *J. Cleaner Prod.* **2017**, *145*, 25−34.

DOI: 10.1021/acs.analchem.9b03268
Anal. Chem. 2019, 91, 13062−13070